Hyperpolarizability density analysis of the enhancement of second hyperpolarizability of ?-conjugated oligomers by intermolecular interaction

ARTICLE *in* INTERNATIONAL JOURNAL OF QUANTUM CHEMISTRY · NOVEMBER 2004

Impact Factor: 1.43 · DOI: 10.1002/qua.20378

6 AUTHORS, INCLUDING:

Masayoshi Nakano
Osaka University
337 PUBLICATIONS **4,785** CITATIONS
SEE PROFILE

Ryohei Kishi
Osaka University
110 PUBLICATIONS **1,948** CITATIONS
SEE PROFILE

Benoît Champagne
University of Namur
401 PUBLICATIONS **8,737** CITATIONS
SEE PROFILE

Edith Botek
Belgian Institute for Space Aeronomy
104 PUBLICATIONS **2,283** CITATIONS
SEE PROFILE

Hyperpolarizability Density Analysis of the Enhancement of Second Hyperpolarizability of π-Conjugated Oligomers by Intermolecular Interaction

MASAYOSHI NAKANO,[1] RYOHEI KISHI,[1] TOMOSHIGE NITTA,[1] BENOÎT CHAMPAGNE,[2] EDITH BOTEK,[2] KIZASHI YAMAGUCHI[3]

[1]*Division of Chemical Engineering, Department of Materials Engineering Science, Graduate School of Engineering Science, Osaka University, Toyonaka, Osaka 560-8531, Japan*

[2]*Laboratoire de Chimie Théorique Appliquée Facultés Universitaires Notre-Dame de la Paix, Namur, Belgium*

[3]*Department of Chemistry, Graduate School of Science, Osaka University, Toyonaka, Osaka, Japan*

Received 30 July 2004; accepted 30 July 2004
Published online 17 November 2004 in Wiley InterScience (www.interscience.wiley.com).
DOI 10.1002/qua.20378

ABSTRACT: In a previous paper we found that the cofacial intermolecular π–π orbital interaction in stacking dimers significantly changes the longitudinal second hyperpolarizability (γ) of the isolated monomer. On the basis of this result, we investigate the longitudinal γ values of π-conjugated main chains (C_nH_{n+2}, $6 \leq n \leq 16$) interacting in both-end regions with two small-size cationic perturbing π-conjugated molecules, that is, allyl cations ($C_3H_5^+$). These interacting model systems exhibit remarkable enhancement of γ values as compared with those of isolated main chains in the whole chain-length region. The γ density analysis reveals that this enhancement is described by the virtual charge transfer between both-end perturbing molecules via the main chain. The analysis of orbital correlation diagram between the perturbing molecules and main chain molecule also clarifies that such feature of γ density distribution originates in the "weak intermolecular antibondinglike coupling" between the (lowest unoccupied molecular orbital [LUMO], LUMO+1) of cationic perturbing molecules and (highest unoccupied molecular orbital [HOMO], HOMO−1) of main chain molecule. The current result suggests the possibility of novel nano-size control of nonlinear optical (NLO) properties by adjusting the intermolecular orbital interactions between the main molecule and perturbing molecules. A possible control scheme of longitudinal γ for novel intermolecular interacting NLO systems using modified DNA wires is also proposed. Int J Quantum Chem 102: 702–710, 2005

Key words: hyperpolarizability; intermolecular interaction; π-conjugated system; DNA; nonlinear optics

Correspondence to: M. Nakano; e-mail: mnaka@cheng.es.osaka-u.ac.jp

Contract grant sponsor: Japan Society for the Promotion of Science.
Contract grant number: 14340184.
Contract grant sponsor: Interuniversity Attraction Pole.
Contract grant number: P5-03.

Introduction

Although the intermolecular interaction effects on the nonlinear optical (NLO) properties are known to be important, for example, through the control of conformation among monomers in macroscopic crystals [1], there have been a few studies on the active control of NLO properties of clusters or crystals by adjusting the intermolecular interactions such as intermolecular charge transfer (CT) and orbital overlap interaction [2–9]. In our previous paper [10], we elucidated that the intermolecular (cofacial) π–π orbital interactions significantly change the magnitude of the longitudinal second hyperpolarizability (γ), which is the microscopic origin of the third-order NLO properties, of isolated monomers using the π–π stacking dimer models composed of $C_5H_7^+$ molecules. On the basis of this result, we have also proposed a novel scheme for enhancing the longitudinal γ of a main π-conjugated chain due to orbital interactions in both-end regions of the main chain with two small-size perturbing molecules [10]. To confirm this speculation, in this study, we examine the effects of intermolecular interactions on γ for coupled systems composed of a main chain molecule, that is, a π-conjugated oligomer (C_nH_{n+2}, $6 \le n \le 16$), interacting in both-end regions with cationic π-conjugated molecules, that is, allyl cations ($C_3H_5^+$). The longitudinal static γ values, which are good approximations to off-resonant γ values, are calculated by the finite-field (FF) approach using the ab initio Hartree–Fock (HF) and Møller-Plesset second-order perturbation (MP2) methods. By comparing γ values among isolated main chains, isolated allyl cations, and interacting systems, we clarify the intermolecular interaction effects on γ as well as on the chain-length dependence of γ. The intermolecular interaction effects are also analyzed in real space using the hyperpolarizability density [11–15], which can reveal the spatial contributions of electrons to hyperpolarizability, and the orbital correlation diagram. On the basis of the current results, we discuss the possibility of novel tunable NLO systems using the intermolecular orbital interactions between the main molecule and perturbing molecules.

Methodology

CALCULATED SYSTEMS AND CALCULATION METHODS

Figure 1 shows the structure of an example of coupled system composed of a main chain (C_nH_{n+2}, $6 \le n \le 16$) (**M**) and two small-size cationic perturbing π-conjugated molecules (allyl cations, $C_3H_5^+$). The main chain lies in x–y plane (molecular plane), whereas the two allyl cations lie in two planes located, respectively, 3.0 Å (van der Waals radius) above and below the molecular plane of main chain. These structural features lead to cofacial π–π orbital interactions in the stacking direction between the main chain and the perturbing molecules at both chain extremities. The geometry of each monomer is optimized under the C_{2v} symmetry for allyl action and C_{2h} symmetry for the main chain C_nH_{n+2} using a hybrid density functional theory (DFT) method, that is, Becke's three-parameter exchange functional and the gradient-corrected functional of Lee, Yang, and Paar (B3LYP) [16, 17] method with the 6-31G** basis set, which is known to reproduce the geometry of polyene chains calculated by the ab initio molecular orbital (MO) methods involving electron-correlation effects [18]. The coupled systems are assumed to be built with the C_i symmetry by simply assembling these monomers, because the effects of the geometry relaxation caused by the intermolecular interaction are negligible for our purpose. All calculations are performed by using Gaussian 98 program package [19].

It is well known that extended basis sets augmented by diffuse and polarization functions (d and p) are at least necessary for reproducing qualitative γ values for small-size hydrocarbon compounds, whereas the basis set dependences are reduced for the longitudinal component of γ of larger-size sys-

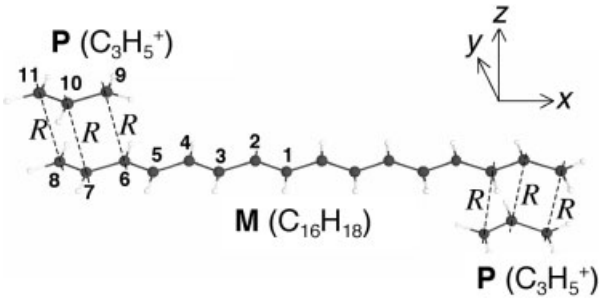

FIGURE 1. Example [$C_{16}H_{18} + 2C_3H_5^+$ (**M** + **2P**)] of model systems composed of a main chain molecule **M** (C_nH_{n+2}, $6 \le n \le 16$) and two cationic perturbing molecules **P** (allyl cation, $C_3H_5^+$). Gray and white circles represent carbon (C) and hydrogen (H) atoms, respectively. The intermolecular distance (R) between **P** and **M** is fixed to be 3.0 Å. The geometry of each monomer (**M** and **P**) is optimized under the C_{2v} symmetry for $C_3H_5^+$ and C_{2h} symmetry for the main chain C_nH_{n+2} using the B3LYP method with the 6-31G** basis set. The coupled system has the C_i symmetry.

tems [20–23]. In our previous study [10], we found that the longitudinal components of γ for monomer ($C_5H_7^+$) and π–π stacking dimers using the 6-31G**+*pd* ($\zeta_{p,d}$ = 0.0523) basis set are in good agreement with those by the 6-31G** basis set, respectively, although the γ values calculated using the 6-31G**+*pd* basis set are slightly (16–18%) enhanced compared with those obtained using the 6-31G** basis set. Therefore, we employ the standard split-valence basis set, 6-31G**, to evaluate the qualitative or semiquantitative variations in the longitudinal γ (γ_{xxxx}) for the model systems in this study. In addition to the HF calculations, the electron correlation effects are assessed by employing the MP2 method, which is known to provide semiquantitative chain-length dependences of γ in π-conjugated linear chains [24–26].

Within the FF approach, the γ_{xxxx} value is calculated numerically as the fourth-order derivative of the total energy E with respect to the applied field:

$$\gamma_{xxxx} = \{E(3F^x) - 12E(2F^x) + 39E(F^x) - 56E(0) + 39E(-F^x) - 12E(-2F^x) + E(-3F^x)\}/\{36(F^x)^4\}. \quad (1)$$

Here, $E(F^x)$ indicates the total energy in the presence of the field F applied in the x direction. An accuracy on γ_{xxxx} of the order of 1% or better is obtained by using a F^x value of 0.001 a.u.

SECOND HYPERPOLARIZABILITY DENSITY ANALYSIS

Before explaining the procedure of hyperpolarizability density analysis, we briefly introduce the usefulness of this analysis. The real-space analysis based on the hyperpolarizability density provides effective measures for the investigation of the mechanism of NLO phenomena and the extraction of molecular design rule for novel NLO materials, because it can reveal, for example, the spatial contribution of substitution groups and the degree of π-conjugation to hyperpolarizability. Although this analysis is usually applied to the static hyperpolarizability based on the FF calculations, it has also been extended to the time-dependent case, in which the hyperpolarizability density can be partitioned into each virtual excitation process [13, 14]. The nonperturbative approach based on the numerical Liouville approach (NLA) [27–29] and the analytical formula of hyperpolarizability density [14] based on the Orr–Ward formula [30] can also be applied to the near-resonant and on-resonant hyperpolarizabilities. Moreover, this analysis is useful for examining the dependence of hyperpolarizability on the levels of approximation, for example, electron correlation level and/or the quality of basis sets in the ab initio molecular orbital (MO), DFT, and semiempirical MO methods.

We here explain the concept of static second hyperpolarizability (γ) density analysis in the FF approach. The charge density function $\rho(\boldsymbol{r}, \boldsymbol{F})$ can be expanded in powers of the field $\boldsymbol{F}$ as [12, 31]

$$\rho(\boldsymbol{r}, \boldsymbol{F}) = \rho^{(0)}(\boldsymbol{r}) + \sum_j \rho_j^{(1)}(\boldsymbol{r}) F^j + \frac{1}{2!}\sum_{jk} \rho_{jk}^{(2)}(\boldsymbol{r}) F^j F^k + \frac{1}{3!}\sum_{jkl} \rho_{jkl}^{(3)}(\boldsymbol{r}) F^j F^k F^l + \ldots . \quad (2)$$

From this equation and the following expansion formula for the dipole moment in a power series of the electric field (in atomic units):

$$\mu^i(\boldsymbol{F}) = -\int \boldsymbol{r}^i \rho(\boldsymbol{r}, \boldsymbol{F}) d\boldsymbol{r}^3 = \mu_0^i + \sum_j \alpha_{ij} F^j + \sum_{jk} \beta_{ijk} F^j F^k + \sum_{jkl} \gamma_{ijkl} F^j F^k F^l + \ldots , \quad (3)$$

the static γ can be expressed by [12]

$$\gamma_{ijkl} = -\frac{1}{3!}\int \boldsymbol{r}^i \rho_{jkl}^{(3)}(\boldsymbol{r}) d\boldsymbol{r}^3, \quad (4)$$

where

$$\rho_{jkl}^{(3)}(\boldsymbol{r}) = \left.\frac{\partial^3 \rho}{\partial F^j \partial F^k \partial F^l}\right|_{F=0}. \quad (5)$$

This third-order derivative of the electron density with respect to the applied electric fields, $\rho_{jkl}^{(3)}(\boldsymbol{r})$, is further referred to as the γ density. In this study, we focus on the longitudinal γ density ($\rho_{xxx}^{(3)}(\boldsymbol{r})$), which is referred to as $\rho^{(3)}(\boldsymbol{r})$. The positive and negative γ density values multiplied by F^3 correspond, respectively, to the field-induced increase and decrease in the charge density (in proportion to F^3), which induce the third-order dipole moment (third-order polarization) in the direction from positive to negative γ densities. Therefore, the γ density map represents the relative phase and magnitude of change

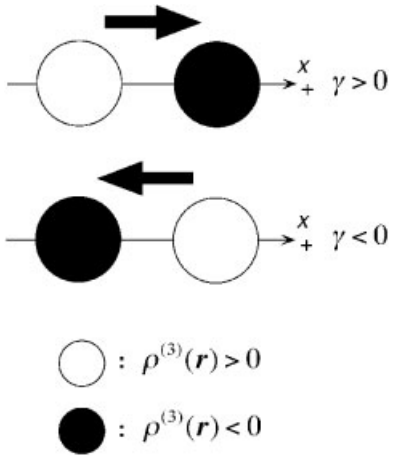

FIGURE 2. Schematic diagram of the second hyperpolarizability (γ) densities [$\rho^{(3)}(\boldsymbol{r})$]. White and black circles represent positive and negative values of $\rho^{(3)}(\boldsymbol{r})$, respectively. The circle size represents the magnitude of $\rho^{(3)}(\boldsymbol{r})$, and the arrow shows the sign of $\rho^{(3)}(\boldsymbol{r})$ determined by the relative spatial configuration between the two $\rho^{(3)}(\boldsymbol{r})$ values.

in the third-order charge densities between two spatial points with positive and negative values. The γ densities are calculated for a grid of points using a numerical third-order differentiation of the electron densities calculated by Gaussian 98.

In order to explain the analysis procedure using γ density map, let us consider a pair of localized γ densities ($\rho^{(3)}(\boldsymbol{r})$) with positive and negative values (see Fig. 2). The sign of the γ contribution is positive when the direction from positive to negative γ density coincides with the positive direction of the coordinate system. The sign becomes negative in the opposite case. Moreover, the magnitude of the γ contribution associated with this pair of γ densities is proportional to the distance between them.

Results and Discussion

LONGITUDINAL γ VALUES OF THE ISOLATED ALLYL CATION AND ISOLATED MAIN CHAINS C_nH_{n+2}

We first examine the longitudinal γ value for the isolated perturbing molecule (allyl cation $C_3H_5^+$) shown in Figure 1. This molecule is found to have a large contribution of symmetric resonance structure with invertible polarization (SRIP) [32], which is a condition of providing negative off-resonant γ due to the relative enhancement of the virtual excitation process referred to as type II [12, 32, 33]. Indeed, the longitudinal γ value for allyl cation at the HF level is found to be -639 a.u., whereas including electron correlation at the MP2 level leads to a 81% increase of the γ magnitude (-1158 a.u. at the MP2 level). Further higher-order electron correlation methods, for example, coupled-cluster method including single, double, and perturbative triple excitations [CCSD(T)], are also known to provide negative γ values (~ -1500 a.u. at the CCSD(T) level using the 6-31G*+*pd* basis set) [34].

The isolated main chain molecules (C_nH_{n+2}) possess positive γ_{xxxx} values displaying a large chain-length dependence of γ at both the HF and MP2 levels. As seen from Figure 3, the MP2 γ values are about 200% larger than their HF analogs for the whole chain-length region, in agreement with similar investigations [26, 35]. Moreover, both methods provide similar nonlinear chain-length dependence of γ.

From these results, even for the smallest isolated main chain, C_6H_8, considered in this study, the magnitude of the main chain γ value (20970 a.u. at the MP2 level) is about 18 times as large as that of the allyl cation (-1160 a.u. at the MP2 level). This indicates that the longitudinal γ for the coupled model shown in Figure 1 would be dominated by that of main chain molecule, if the intermolecular interactions were ignored. Such γ feature for the

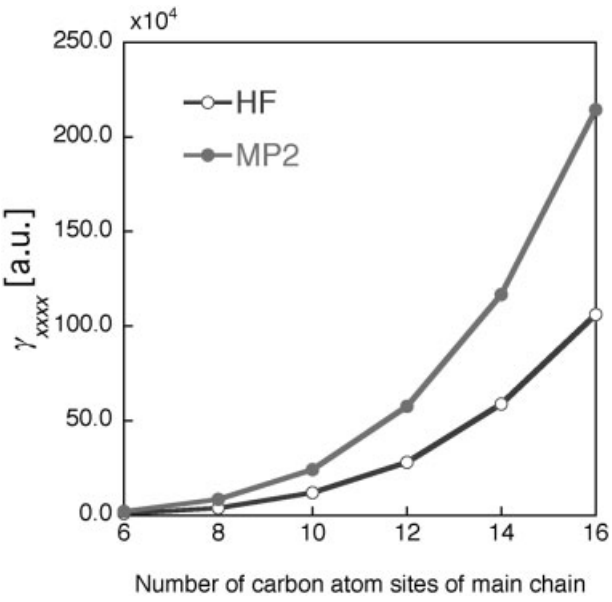

FIGURE 3. Chain-length dependences of longitudinal γ of isolated main chains **M** (C_nH_{n+2}, $6 \leq n \leq 16$) at the HF and MP2 levels.

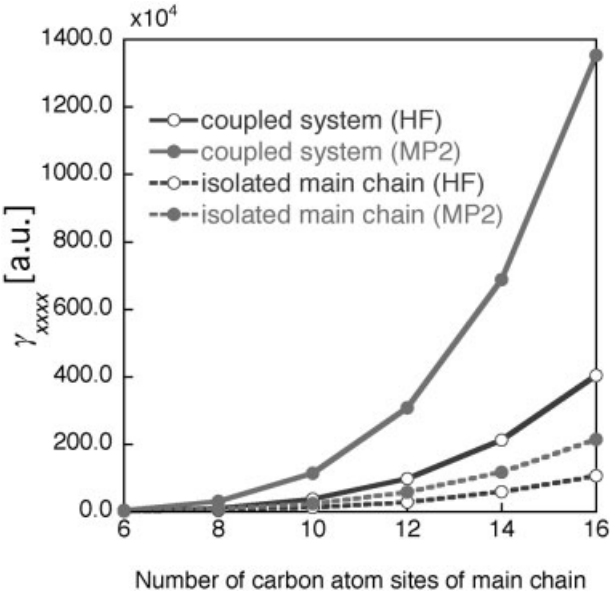

FIGURE 4. Chain-length dependences of longitudinal γ of coupled systems (**M** + **2P**) and isolated main chains **M** (C_nH_{n+2}, $6 \leq n \leq 16$) at the HF and MP2 levels.

allyl cation is consistent with its status of perturbing molecules in the couple systems.

INTERMOLECULAR INTERACTION EFFECTS ON THE LONGITUDINAL γ VALUES OF COUPLED SYSTEMS COMPOSED OF TWO ALLYL CATIONS AND A MAIN CHAIN C_nH_{n+2}

In the following, we discuss the results obtained at the HF and MP2 levels with the 6-31G** basis set. Figure 4 shows the chain-length dependences of the longitudinal γ values for the coupled systems in comparison to those of the isolated main chains. The HF and MP2 γ values for both coupled systems and isolated main chains show significant chain-length dependences. For any chain length, the MP2 γ value of the isolated main chain is about two times larger than the corresponding HF γ value, whereas for coupled systems the MP2 γ value is about three times larger. This shows that the electron correlation effects are more important to estimate γ values and their chain-length dependence for interacting systems than for the isolated systems. Moreover, the enhancement factor x, defined by the (γ value for coupled system)/(γ value for isolated main chain) ratio, increases with chain length: $x = 2.00$ ($n = 4$), $x = 4.72$ ($n = 10$), and $x = 6.31$ ($n = 16$) at the MP2 level. This is a substantial enhancement, which deserves to be understood in view of designing γ-based NLO materials. It can be associated with the modifications of the charge distributions of the allyl cations and the main chain. The main chain can be considered as a polyacetylene segment end-capped by two acceptor groups. Indeed, the allyl cations induce a charge transfer from the main chain to the allyl cations, which amounts to 0.393 per one allyl cation (0.169 on site **11**, 0.004 on site **10**, and 0.220 on site **9**; see Fig. 1) at the MP2 level, whereas the corresponding positive charge (2×0.393) is distributed in relatively delocalized manner in the whole chain region: 0.092 on site **8**, 0.027 on site **7**, 0.032 on site **6**, 0.069 on site **5**, 0.025 on site **4**, 0.062 on site **3**, 0.036 on site **2**, and 0.049 on site **1** at the MP2 level. As a result, in the coupled system, each carbon atom site of the main chain is slightly positive: 0.052 on site **8**, 0.064 on site **7**, 0.035 on site **6**, 0.069 on site **5**, 0.026 on site **4**, 0.062 on site **3**, 0.037 on site **2**, and 0.049 on site **1** at the MP2 level. Following recent studies, symmetric substitution by acceptor groups enhances the third-order NLO response of polyacetylene chains [23, 36]. Despite such charge redistribution (CT from the main chain to allyl cations), both allyl cations possess a positive charge of 0.6075 while the main chain positive charge (0.786) is distributed on each carbon atom site. This feature enables us to speculate that the virtual CT between both-end allyl cations through the main chain causes the remarkable enhancement of the third-order hyperpolarization because each allyl cation and the end region of main chain interact with each other through π–π orbital overlap. In order to verify our speculation, we examine the γ density distributions of these systems in the next section.

γ Density Analysis of Isolated Allyl Cation, Isolated Main Chain, and Coupled System

The longitudinal γ densities of isolated allyl cation (a), isolated main chain $C_{16}H_{18}$ (b), and the coupled system, $C_{16}H_{18}$ interacting with two allyl cations (c) at the MP2 level are shown in Figure 5. The isolated allyl cation provides a negative γ, which is primarily associated with the virtual CT between both-end π-electron distributions [see Fig. 5(a)]. The main chain, $C_{16}H_{18}$, exhibits large positive and negative π-electron γ densities distributed on the left and right sides, respectively, which leads

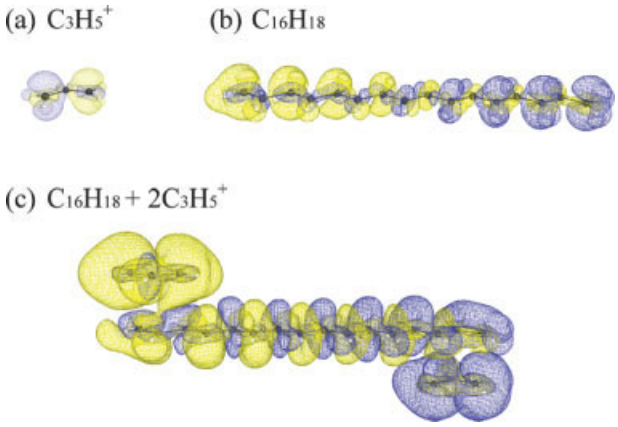

FIGURE 5. Isosurfaces of longitudinal MP2 γ densities of isolated allyl cation ($C_3H_5^+$) (a), isolated main chain ($C_{16}H_{18}$) (b), and the coupled system ($C_{16}H_{18}$ + $2C_3H_5^+$) (c). The yellow and blue meshes represent the isosurfaces with 20 a.u. (1000 a.u.) and −20 a.u. (−1000 a.u.), respectively, for (a) [(b) and (c)].

to a positive longitudinal γ, although the π-electron γ densities distribute on alternate sites [see Fig. 5(b)]. Figure 5(b) also shows that the σ-electron γ densities go in the opposite direction, although their contributions are smaller than π-electron contributions, slightly reducing therefore the global hyperpolarization. In the coupled system, the allyl cation on the left side exhibits positive π-electron γ densities, whereas that on the right side exhibits negative π-electron γ densities. In the main chain region, we observe larger magnitudes of π-electron γ densities, in which positive and negative γ densities are again alternately distributed, than those for the isolated main chain [see Fig. 5(b, c)]. Judging from the positive (left) and negative (right) π-electron γ densities of the allyl cations in the coupled system, the virtual CT between both-end allyl cations via the main chain is predicted to contribute to the enhancement of γ for the coupled system.

RELATION BETWEEN γ AND THE ORBITAL CORRELATION BETWEEN MAIN CHAIN AND TWO ALLYL CATIONS

In order to understand the features of γ density distributions in the coupled systems, we investigate the MO correlation diagram for the coupled system [$C_{16}H_{18}$ + $2C_3H_5^+$ (**M** + **2P**)] at the HF level (see Fig. 6). The central diagram shows the orbitals for the coupled system whereas the diagrams at both ends show the orbitals for the isolated main chain (**M**) and both-end allyl cations (**2P**), respectively. The orbitals of these systems belong to the gerade(**g**) or ungerade(**u**) symmetry with respect to the inversion center of the system. The lowest unoccupied molecular orbital (LUMO) and LUMO+1 of **2P** correspond to the gerade(**g**) and ungerade(**u**) mixings of LUMOs of the two allyl cations, respectively. The LUMO(**g**) and LUMO+1(**u**) of **2P** are nearly degenerate, whereas their spatial distribution is almost identical to the LUMO(**g**) of the isolated allyl cation because of the slight interaction between remote both-end allyl cations. As a result of the MO symmetry and occupation numbers of **2P** and **M**, the important interactions occur between the LUMO(**g**) and LUMO+1(**u**) of **2P** on the one hand and the highest occupied molecular orbital (HOMO) (**g**) and HOMO−1(**u**) of **M**, on the other hand. From these interactions, four levels are formed of which two are doubly occupied. The latter, the HOMO(**g**) and HOMO−1(**u**) of the coupled systems, are in fact stabilized by the intermolecular bondinglike interactions in both-end regions. The energy spacing between these occupied levels is almost identical to the spacing between the parent MOs of **M** [HOMO(**g**) and HOMO−1(**u**)]. On the other hand,

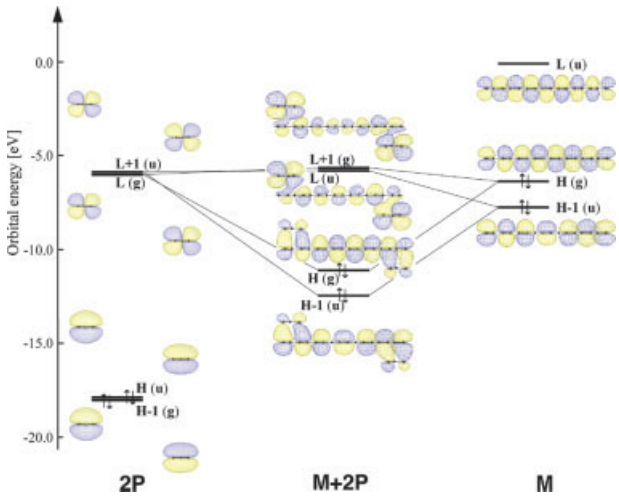

FIGURE 6. Orbital correlation diagrams of the coupled system [$C_{16}H_{18}$ + $2C_3H_5^+$ (**M** + **2P**)], which is shown in the center, and both ends show those for **2P** and **M**, which denotes isolated perturbing molecules (two allyl cations, $2C_3H_5^+$) and an isolated main chain ($C_{16}H_{18}$), respectively. Isosurfaces (yellow mesh for 0.01 a.u. and blue mesh for −0.01 a.u.) of MOs are also shown. Symbols **H** and **L** represent the HOMO and LUMO, respectively, and symbols **g** and **u** denote the gerade and ungerade orbitals with respect to the inversion center of the system, respectively.

the orbital energies of the LUMO(**u**) and LUMO+1(**g**) of the coupled systems are nearly identical and equal to those of **2P**. These MOs are dominated by the LUMO+1(**u**) and LUMO(**g**) of **2P**. This feature can be understood by the fact that the intermolecular antibondinglike interaction between **2P** and **M** in both-end regions is weakened by the partial intermolecular bondinglike mixing [see LUMO(**u**) and LUMO+1(**g**) of the coupled system shown in Fig. 6]. As a result, although the HOMO–LUMO gap of the coupled system is nearly equal to that (~5.2 eV) of the main chain, the LUMO–LUMO+1 gap (~0.16 eV) of the coupled system is much smaller than that (~3.7 eV) of the main chain. Such features are expected to be realized when (i) the orbital energies of [LUMO(**g**), LUMO+1(**u**)] for cationic perturbing molecules are near to those of [HOMO(**g**), HOMO−1(**u**)] for main chain and (ii) "weak orbital coupling" exist between these MOs. This LUMO–LUMO+1 gap and orbital transition moment between the LUMO and LUMO+1 of the coupled system approximately correspond to the transition energy and transition moment between the first and the second excited states of the coupled system, respectively. The transition density between the LUMO and LUMO+1 exhibits the positive and negative transition densities on the left and right side allyl cations, respectively, which implies the large contribution of both-end allyl cations to the transition moment, because the transition moment is determined by a pair of positive and negative transition densities, and its magnitude increases as a function of the distance between the positive and negative transition densities and their magnitudes. These features cause the enhancement of γ through the type III virtual excitation process [32, 33] involving the excitation between the first and second excited states. The transition density between the LUMO and LUMO+1 and that between the HOMO and LUMO of the coupled system also support the γ density distribution of the coupled system shown in Figure 5(c). This can be understood as follows. The γ density for the type III process, which is predicted to be dominant in the current system due to the small energy gap between LUMO and LUMO+1, is composed of two parts. The first involves the transition density $[\rho_{g,e1}(r)]$ between the ground (g) and the first (e1) excited states, whereas the second involves that $[\rho_{e1,e2}(r)]$ between the first (e1) and second (e2) excited states [37]. Because in this case, the first and second excited states are approximately described by the orbital transition from HOMO to LUMO and that from HOMO to LUMO+1, the transition densities $\rho_{g,e1}(r)$ and $\rho_{e1,e2}(r)$ are approximately described by the orbital transition densities $\rho_{HOMO,LUMO}(r)$ and $\rho_{LUMO,LUMO+1}(r)$, respectively. Indeed, the features, for example, relative phase, for these transition densities well represent those of γ densities shown in Figure 5(c). In conclusion, the enhancement of γ for the coupled system is ascribed to be the weak intermolecular antibondinglike interaction between the [LUMO(**g**), LUMO+1(**u**)] of **2P** and [HOMO(**g**), HOMO−1(**u**)] of **M** because this provides the near degenerate LUMO(**u**) and LUMO+1(**g**) of the coupled system, which dominantly involve the LUMO+1(**u**) and LUMO(**g**) of both-end allyl cations, respectively. Such enhancement mechanism is similar to that of the two-photon absorption (TPA) for the symmetric systems including the both-end cationic groups linked with a π-conjugated bridge [38]. Therefore, the orbital interaction between the main chain and the anionic perturbing molecules instead of cationic ones is speculated to provide similar enhancement of γ due to the near-degenerate HOMO and HOMO−1 orbitals of coupled systems.

Conclusion

Using the ab initio HF and MP2 methods, we have investigated the intermolecular interaction effects of the longitudinal γ for the coupled systems composed of a π-conjugated main chain molecule, C_nH_{n+2} ($6 \le n \le 16$), and the two cationic perturbing π-conjugated molecules, allyl cations, $C_3H_5^+$, located in both end regions, respectively. The longitudinal γ values of the coupled systems are remarkably enhanced, as are their chain-length dependences with respect to those of isolated main chains. These enhancements turn out to be described by the virtual CT between both-end perturbing molecules via the main chain using the γ density analysis. This feature is predicted to be caused by the weak intermolecular antibondinglike coupling between the (LUMO, LUMO+1) for cationic perturbing molecules and (HOMO, HOMO−1) for a main chain molecule.

A possibility to control the γ enhancement is sketched in Figure 7. Indeed, because the NLO response is sensitive to the positions of the perturbing molecules as well as the distances between them, well-defined structural parameters can be

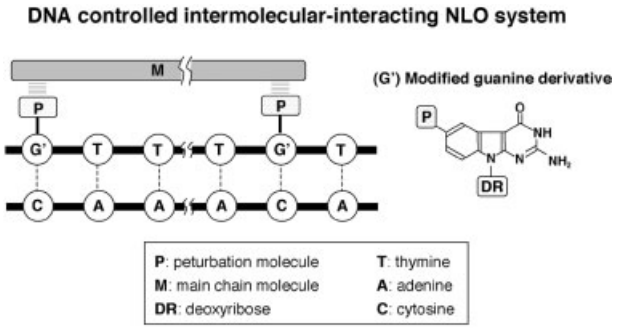

FIGURE 7. Schematic diagram of DNA-controlled intermolecular-interacting NLO system. Letters **M** and **P** depict the main chain and perturbing molecule, respectively. Letters **T**, **A**, **C**, and **G′**, respectively, indicate thymine, adenine, cytosine, and modified guanine, in which oxidative damage is protected and involves the perturbing group, for example, $C_3H_5^+$.

fixed by using a modification of DNA wires. In this model, the perturbing molecules are introduced into the modified guanine derivative [39], in which the oxidative damage is protected by the modification of structure of guanine [see Fig. 7(G′)], and the positions of perturbing molecules are controlled by adjusting the sequence of base pairs.

The current investigation clarifies the enhancement mechanism of the longitudinal γ in coupled systems due to intermolecular orbital interactions in both-end regions between cationic molecules and a main chain molecule. As predicted from the analysis of the correlation MO diagram, the relative position of the perturbing molecules could modulate the degree of the enhancement of γ. Such novel control scheme of NLO properties will be realized using the structural control of nano-size molecular systems, for example, modified DNA wires.

ACKNOWLEDGMENTS

This work was supported by Grant-in-Aid for Scientific Research (no. 14340184) from Japan Society for the Promotion of Science (JSPS). One of the authors (E. B.) thanks the Interuniversity Attraction Pole on "Supramolecular Chemistry and Supramolecular Catalysis" (IUAP no. P5-03) for her postdoctoral grant. One of the authors (B. C.) thanks the Belgian National Fund for Scientific Research for his Senior Research Associate position.

References

1. Champagne, B.; Bishop, D. M. Adv Chem Phys 2003, 126, 41.
2. Nakano, M.; Yamaguchi, K.; Fueno, T. Kobunshi Ronbunshu 1990, 47, 779.
3. Nakano, M.; Yamaguchi, K.; Fueno, T. In Computer Aided Innovation of New Materials; Doyama, M.; Suzuki, T.; Kihata, J.; Yamamoto, R., Eds.; Elsevier: Amsterdam, 1991; p 259.
4. Gotoh, T.; Kondoh, T.; Egawa, K. J Opt Soc Am B 1990, 6, 703.
5. Nakano, M.; Yamaguchi, K.; Fueno, T. Nonlinear Optics 1994, 6, 289.
6. Nakano, M.; Yamada, S.; Yamaguchi, K. Chem Phys Lett 1999, 311, 221.
7. Nakano, M.; Yamada, S.; Yamaguchi, K. J Phys Chem A 1999, 103, 3103.
8. Kisida, H.; Matsuzaki, H.; Okamoto, H.; Manabe, T.; Yamashita, M.; Taguchi, Y.; Tokura, Y. Nature 2000, 405, 929.
9. Ottonelli, M.; Musso, G. F.; Comoretto, D.; Dellepiane, G. Phys Chem Chem Phys 2002, 4, 2754.
10. Nakano, M.; Yamada, S.; Takahata, M.; Yamaguchi, K. J Phys Chem A 2003, 107, 4157.
11. Nakano, M.; Yamaguchi, K.; Fueno, T. Chem Phys Lett 1991, 185, 550.
12. Nakano, M.; Shigemoto, I.; Yamada, S.; Yamaguchi, K. J Chem Phys 1995, 103, 4175.
13. Nakano, M.; Yamada, S.; Shigemoto, I.; Yamaguchi, K. Chem Phys Lett 1996, 250, 247.
14. Nakano, M.; Fujita, H.; Takahata, M.; Yamaguchi, K. Chem Phys Lett 2002, 356, 462.
15. Nakano, M.; Nagao, H.; Yamaguchi, K. Phys Rev 1997, A55, 1503.
16. Becke, A. D. J Chem Phys 1993, 98, 5648.
17. Lee, C.; Yang, W.; Parr, R. G. Phys Rev B 1988, 37, 785.
18. Perpète, E. A.; Champagne, B. J Mol Struct (Theochem) 1999, 487, 39; Champagne, B.; Spassova, M. Phys Chem Chem Phys 2004, 6, 3167.
19. Frisch, M. J.; Trucks, G. W.; Schlegel, H. B.; Scuseria, G. E.; Robb, M. A.; Cheeseman, J. R.; Zakrzewski, V. G.; Montgomery, J. A.; Stratmann, R. E.; Burant, J. C.; Dapprich, S.; Millam, J. M.; Daniels, A. D.; Kudin, K. N.; Strain, M. C.; Farkas, O.; Tomasi, J.; Barone, V.; Cossi, M.; Cammi, R.; Mennucci, B.; Pomelli, C.; Adamo, C.; Clifford, S.; Ochterski, J.; Petersson, G. A.; Ayala, P. Y.; Cui, Q.; Morokuma, K.; Malick, D. K.; Rabuck, A. D.; Raghavachari, K.; Foresman, J. B.; Cioslowski, J.; Ortiz, J. V.; Stefanov, B. B.; Liu, G.; Liashenko, A. P.; Piskorz, A. P.; Komaromi, I.; Gomperts, R.; Martin, R. L.; Fox, D. J.; Keith, T.; Al-Laham, M. A.; Peng, C. Y.; Nanayakkara, A.; Gonzalez, C.; Challacombe, M.; Gill, P. M. W.; Johnson, B. G.; Chen, W.; Wong, M. W.; Andres, J. L.; Head-Gordon, M.; Replogle, E. S.; Pople, J. A. Gaussian 98, Revision A.11; Gaussian: Pittsburgh, 1998.
20. Hurst, G. J. B.; Dupuis, M.; Clementi, E. J Chem Phys 1988, 89, 385.
21. Nakano, M.; Fujita, H.; Takahata, M.; Yamaguchi, K. J Am Chem Soc 2002, 124, 9648.

22. Yamada, S.; Nakano, M.; Shigemoto, I.; Yamaguchi, K. Chem Phys Lett 1996, 254, 158.
23. Champagne, B.; Kirtman, B. In Handbook of Advanced Electronic and Photonic Materials and Devices, Vol. 9: Nonlinear Optical Materials; Nalwa, H. S., Ed.; Academic Press; New York, 2001; Chap. 2, p 63.
24. Nakano, M.; Yamada, S.; Yamaguchi, K. Int J Quantum Chem 1998, 70, 269.
25. Toto, J. L.; Toto, T. T.; de Melo, C. P.; Hasan, M.; Kirtman, B. Chem Phys Lett 1995, 224, 59.
26. Champagne, B.; Perpète, E. A.; van Gisbergen, S. J. A.; Snijders, J. G.; Baerends, E. J.; Soubra-Ghaoui, C.; Robins, K. A.; Kirtman, B. J Chem Phys 1998, 109, 10489; erratum 1999, 110, 11664.
27. Nakano, M.; Yamaguchi, K. Phys Rev A 1994, 50, 2989.
28. Nakano, M.; Yamaguchi, K.; Matsuzaki, Y.; Tanaka, K.; Yamabe, T. J Chem Phys 1995, 102, 2986.
29. Nakano, M.; Yamaguchi, K.; Matsuzaki, Y.; Tanaka, K.; Yamabe, T. J Chem Phys 1995, 102, 2996.
30. Orr, J.; Ward, J. F. Mol Phys 1971, 20, 513.
31. Chopra, P.; Carlacci, L.; King, H.; Prasad, P. N. J Phys Chem 1989, 93, 7120.
32. Nakano, M.; Yamaguchi, K. Chem Phys Lett 1993, 206, 285.
33. Nakano, M.; Yamada, S.; Shigemoto, I.; Yamaguchi, K. Chem Phys Lett 1996, 251, 381.
34. Nakano, M.; Yamaguchi, K. Mol Cryst Liq Cryst A 1994, 255, 139.
35. Kirtman, B.; Champagne, B.; Gu, F. L.; Bishop, D. M. Int J Quantum Chem 2002, 90, 709.
36. Meyers, F.; Brédas, J. L. Synth Metals 1992, 49–50, 181; Puccetti, G.; Blanchard-Desce, M.; Ledoux, I.; Lehn, J. M.; Zyss, J. J Phys Chem 1993, 97, 9385.
37. Nakano, M.; Fujita, H.; Takahata, M.; Yamaguchi, K. Chem Phys Lett 2002, 356, 462.
38. Kishi, R.; Nakano, M.; Yamada, S.; Kamada, K.; Ohta, K.; Nitta, T.; Yamaguchi, K. Chem Phys Lett 2004, 393, 437.
39. Okamoto, A.; Tanaka, K.; Saito, I. J Am Chem Soc 2003, 125, 5066.